



ELSEVIER

Available online at [www.sciencedirect.com](http://www.sciencedirect.com)

Remote Sensing of Environment 112 (2008) 1712–1729

---



---

Remote Sensing  
of  
Environment

---



---

[www.elsevier.com/locate/rse](http://www.elsevier.com/locate/rse)

## On the use of the dual-frequency ENVISAT altimeter to determine snowpack properties of the Antarctic ice sheet

P. Lacroix <sup>a,\*</sup>, M. Dechambre <sup>b</sup>, B. Legrésy <sup>a</sup>, F. Blarel <sup>a</sup>, F. Rémy <sup>a</sup>

<sup>a</sup> LEGOS, 14 av. Edouard Belin 31400 Toulouse, France

<sup>b</sup> CETP, 10-12 av. de l'Europe, 78140 Velizy, France

Received 4 June 2007; received in revised form 27 August 2007; accepted 28 August 2007

---

### Abstract

The primary purpose of ice-sheet altimetry is to monitor the changes in ice-sheet topography which may impact on global sea-level. However, the altimetric signal is sensitive to different properties of the snowpack, and therefore can also be used to determine these properties. The radar altimeter onboard the European Space Agency's ENVISAT satellite provides a dual-frequency dataset at Ku (13.6 GHz) and S band (3.2 GHz). In this paper, these signals are studied over the Antarctic ice-sheet during the 4 first years of the mission (2002–2006), in order to retrieve snowpack properties.

The altimeter signal can be described by 4 classical waveform parameters. The 4 year time-series of all these parameters are decomposed into a linear and a seasonal time component. The linear component is almost constant. The distribution of the mean parameters over the Antarctic ice-sheet shows that the altimeter signal is sensitive to small-scale (mm) surface roughness.

For the first time, the amplitudes and phases of the seasonal variations are characterized. The S band amplitudes are greater than the Ku band, and the phase varies over the entire ice-sheet. Previous studies suggested that the seasonal variations of the altitude from the altimeter are created by a decrease of the snowpack height through compaction. The dual-frequency observations shown here suggest that this hypothesis is too simple. Instead, the altitude variations observed in the altimetric signal are not created by the snowpack height change, but are more likely caused by the seasonal change of the snow properties, which cause a different response between the S and Ku bands. Therefore, both the linear and the seasonal variations of the altimetric signal can be used to retrieve snowpack properties.

Here, we compare the dual-frequency ENVISAT signal with a model of the altimetric echo over the Antarctic ice-sheet. The model combines a surface model with a sub-surface model, for both the S and Ku bands. The Brown model [Brown G. S. (1977). The average impulse response of a rough surface and its applications. *IEEE Transactions on Antennas and Propagation*, 25, 1.] is used to describe the interaction of the radar wave with the snow surface. The backscatter coefficient of the surface is derived using the IEM method [Fung, A. K. (1994). *Microwave scattering and emission models and their applications*, Boston, MA: Artech House.]. The sub-surface signal takes into account both the layering effects and the scattering caused by the homogeneous media which is composed of small snow grains. The model is tested in two areas of the Antarctic plateau which present very different waveform parameters. The sensitivity of the radar signal to the different snowpack properties is investigated. The analysis of the waveform behaviours shows that the sub-surface signal can be completely masked by the small-scale surface roughness signal.

Finally, the temperature and surface density effects are investigated in order to explain the seasonal variations of the altimetric signal. Both the temperature and the compaction rate of the snow change seasonally. Temperature is shown to impact on the Ku band signal. Furthermore, the compaction rate of the snow surface can explain all of the seasonal variation characteristics observed at both the S and Ku bands. The seasonal change of compaction rate in the snow creates a change in the waveform shape that can bias the altitude. In particular, the snow compaction can induce a bias in the retrieved altimetric altitude of more than 80 cm for the Ku band and 1.5 m for the S band. This work underlines that the altitude time-series needs to be corrected for the shape of the altimetric echo over ice-sheets.

© 2007 Elsevier Inc. All rights reserved.

*Keywords:* Altimeter; Antarctic ice sheet; Snowpack properties; Snow compaction; Radar modelling

---

\* Corresponding author.

E-mail address: [lacroix@notos.cst.cnes.fr](mailto:lacroix@notos.cst.cnes.fr) (P. Lacroix).

## 1. Introduction

Satellite altimeters are vertical looking radars, developed initially to measure the level of the oceans. They have also been used over ice-sheets in order to monitor their topography (Rémy et al., 1999). The relatively long time-series of altimetric data (8 years of ERS data in the period 1993–2001 and 5 years of ENVISAT data since 2002) have allowed us to monitor interannual changes in topography which may impact on global sea-level (Zwally et al., 2005; Legrésy et al., 2006).

The RA-2 altimeter onboard the European Space Agency's ENVISAT satellite launched in 2002 provides a S band dataset (3.2 GHz), in addition to the classic Ku data band (13.6 GHz). The dual-frequency signal acquired over the Antarctic ice-sheet depends strongly on the different snowpack properties (Legrésy et al., 2005; Lacroix et al., 2007). Radar waves penetrate into the dry snow of the Antarctic plateau. The penetration depth ranges from 5 to 12 m at the Ku band (Legrésy & Rémy, 1998; Lacroix et al., 2007). At lower frequencies there is less extinction of the signal, and the penetration depth at S band is certainly deeper. The scattering of the radar waves is caused by both the snow grain distribution (volume scattering) (Ridley & Partington, 1988; Rémy et al., 2001), and the internal layering within the snowpack (Hawley et al., 2006; Lacroix et al., 2007) created by inhomogeneous snow densities (surface scattering). Internal layering of the snowpack is caused by seasonal snow accumulation and compaction. The altimetric echo depends strongly on the surface topography and the roughness at different scales such as megadunes (10 m in height and over 1 km horizontally) or the sastruggis (1 m in height and over 10 m horizontally) (Legrésy & Rémy, 1997). The snow surface roughness at the centimetric and millimetric scale also has a large impact on the altimetric waveforms (Lacroix et al., 2007). Knowledge of these snow properties is of particular interest because they are indicators of changes in the accumulation rate, the wind strength or the temperature.

The present paper shows how the dual-frequency information provided by the ENVISAT altimeter can be used to retrieve the snowpack properties over the Antarctic ice-sheet. This work is based on an analysis of 4-years of ENVISAT data and a model of the radar altimeter echo based on the Brown model (1977) adapted to the ice-sheet environment.

In Section 2, the 4-year ENVISAT database over the Antarctic ice-sheet is presented. A set of 4 classic waveform parameters are presented. The time-series of each parameter is presented as a superposition of 2 components: a linear time dependent component and a seasonally time dependent component. The linear time dependent component can be considered as a constant value over the 4 years as it varies slowly. In Section 3, the spatial repartition of the mean value over 4 years is analysed for each parameter. This analysis highlights the primary importance of the millimetre snow surface roughness, which impacts on all of the parameters at both the Ku and S bands.

Seasonal variations were first observed by Zwally and Li Jun (2002), in the height time-series. They attributed its origin to the seasonal compaction of the snow in late spring, which causes the height of the snowpack to drop. Here, the seasonal variations of

the 4 dual-frequency parameters are also investigated. Both the amplitude and the phase of the seasonal variations of each parameter are considered. The S band amplitudes are found to be greater than those of the Ku band, and the phase differs over the entire ice sheet. This observation leads us to propose that the seasonal altitude variations are partly due to a change in the waveform shape, which varies with different snow-wave interactions depending on the season and the radar frequency. Therefore the two dual-frequency component analysis can improve our knowledge of the snow properties over the ice-sheets.

Section 4 presents a radar echo model developed to better understand the snow-wave interaction mechanisms. Until now, the radar echo models have been used to retrieve the volume and surface contributions to the altimeter signal (Ridley & Partington, 1988; Davis & Moore, 1993; Legrésy & Rémy, 1997; Arthern et al., 2001) but not the snow properties. Radar echo models have been designed to estimate the error on the altitude retrieval created by the combination of surface and volume scattering (Femenias et al., 1993; Newkirk & Brown, 1996; Wingham, 1995; Adams & Brown, 1998). Furthermore, all of the previous models have been designed for the Ku band. In our study, we adapt the Brown model (1977) in order to use it simultaneously at the S and Ku band. The model is then used to explain the linear and seasonal variations of the waveform parameters. The results are presented in Sections 5 and 6.

## 2. ENVISAT observations

### 2.1. Waveform parameters

The ENVISAT altimeter characteristics are summarized in Table 1. One of its major particularities, in regard to the previous ERS missions, is that it provides simultaneously two datasets at Ku and S bands. The S band was originally designed to correct for ionospheric delays, but can also be used for geophysical studies because it provides a different signal to the Ku band. The altimeter waveform represents the power of the reflected radar echo as a function of the two-way travel time. The time record is 400 ns sampled at 3.125 ns for the Ku band and 6.25 ns for the S band. The two waveforms can then be compared when they are corrected for their specific antenna characteristics, that act on each waveform shape. The correction is applied with the assumption that the altimetric echo is only returned from the surface, that is the wave does not penetrate into the snow. Thus, the echo at time  $t$  in the waveform corresponds to a certain incidence angle  $\theta$  from the satellite (for example, Lacroix et al., 2007). The correction is then

Table 1  
ENVISAT altimetric radar characteristics

Parameter	S band	Ku band
Center frequency $f_0$	3.2 GHz	13.6 GHz
Wavelength $\lambda$	9.4 cm	2.2 cm
Bandwidth $B$	160 MHz	320 MHz
Vertical resolution	94 cm	47 cm
Antenna beamwidth at 3 dB	5.5°	1.35°

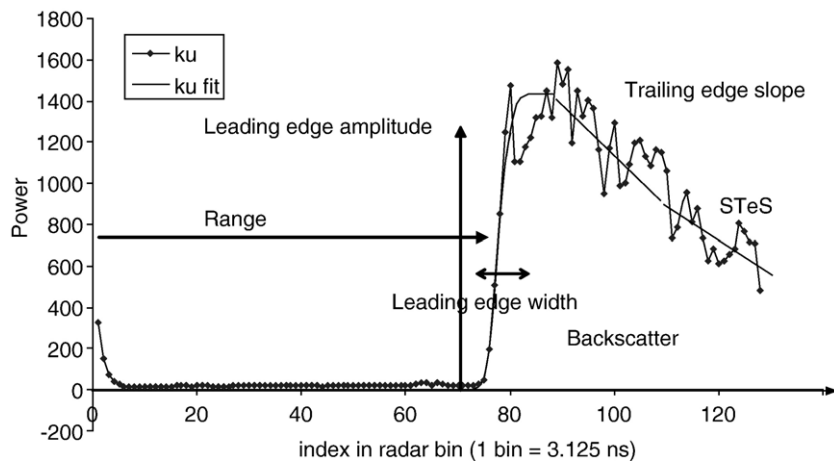


Fig. 1. Altimetric waveform parameters definition.

obtained by multiplying the echo at time  $t$  by the inverse of the antenna gain for the angle  $\theta$ . This correction will give a horizontal trailing edge for a medium with a perfect Lambertian surface.

Four main parameters are derived from the shape of the waveform (Legrésy & Rémy, 1997); These are the range,  $R$  (m), the leading edge width, LeW (m), the trailing edge slope, TeS ( $\text{Np s}^{-1}$ ) and the backscattering coefficient,  $\sigma_0$  (dB) (cf Fig. 1), as given by the Ice2 retracking algorithm (Legrésy et al., 2005). TeS is the slope

of the first 32 radar bins of the waveform trailing edge expressed in a logarithmic scale. A secondary parameter, the second trailing edge slope (STeS) is closely related to TeS and is defined as the slope of the next 32 radar bins of the trailing edge.

Each of the parameters varies as a function of the properties of the illuminated surface and from the sub-surface medium; for example, LeW is related to the local topography, the sastruggi and the wave penetration depth (Legrésy & Rémy, 1997). Also, the S

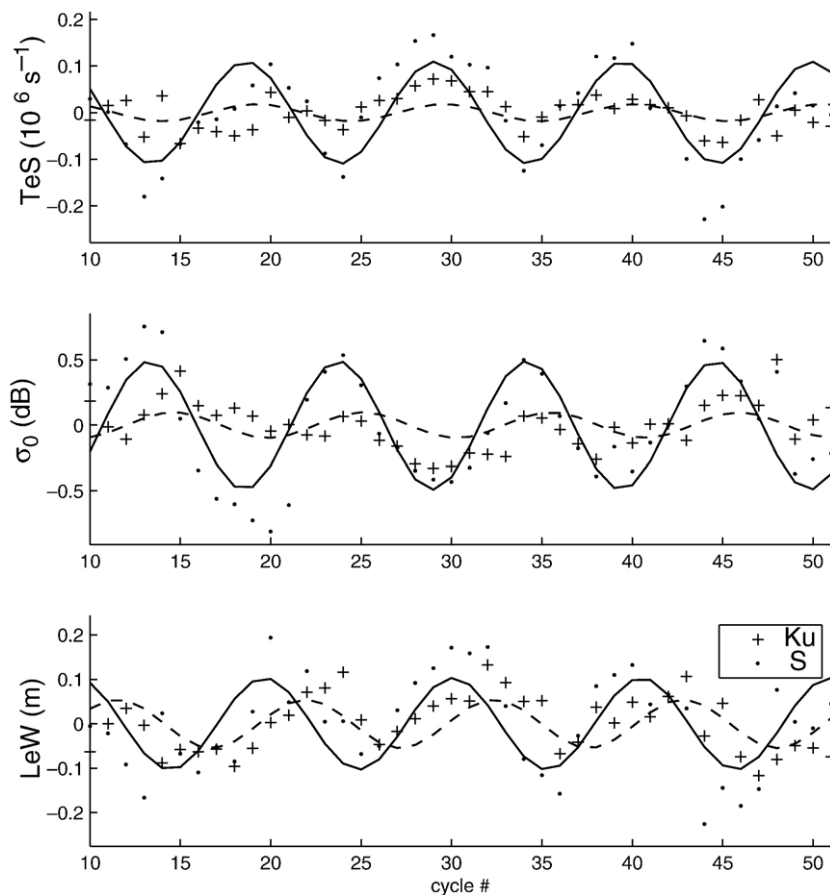


Fig. 2. Time-series of the waveform parameters (from top to bottom: trailing edge slope, backscatter coefficient, and leading edge width). The trend over 4 years is removed. The series show clear seasonal variations of 1 year period.

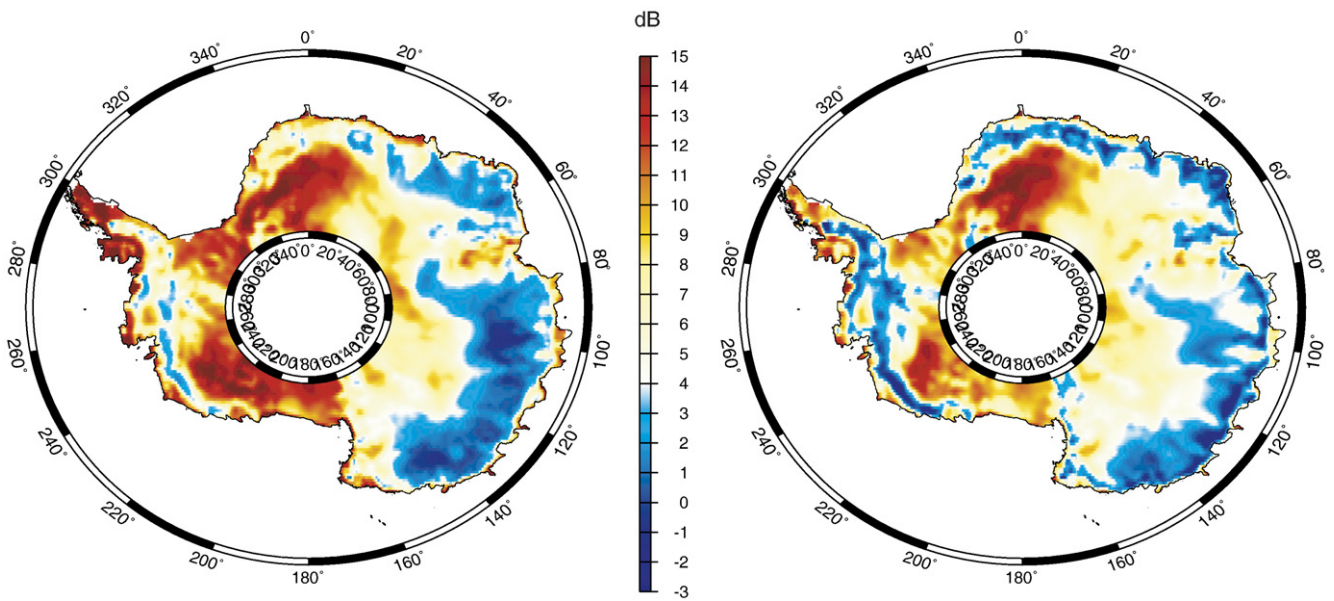


Fig. 3. Backscatter coefficient map over the Antarctica plateau at S (left) and Ku band (right). Unit is dB.

and Ku band penetration property difference leads to a LeW difference which induces an altitude bias (Legrésy et al., 2005). The scattering by snow grains is an important contribution to the Ku sub-surface signal and decreases with respect to the frequency. This can induce different backscattering coefficients between the 2 bands. The trailing edge slope is related to the topographic slope and the penetration depth. The TeS behaviours are described in detail in Section 3.

### 2.2. Processing 4 years of ENVISAT data

In this section we consider 4 years of ENVISAT altimeter data from November 2002 (cycle 9) until December 2006 (cycle 51)

over the Antarctic ice-cap. The data have been divided into cells of  $0.1^\circ$  of latitude by  $0.25^\circ$  of longitude. Most of the waveform parameters remain fairly constant over this cell size, except for the altitude. For each cycle, we average the waveform parameters for all points situated in the same cell. For each cell, a cycle of 35 days produces 10 measurements of every waveform parameter per year (Fig. 2). The mean value over the 4 year period is calculated (Figs. 3, 4 and 5). This confirms a qualitative analysis of the mean dual-frequency signal over 3 months (cycles 9 to 12) by Legrésy et al. (2005). A linear trend is then removed from each time series, but not shown here. A sinusoidal function of 1 year period is then fitted to the time-series (Fig. 2). Its amplitude is mapped in Figs. 6, 7, 8 and its phase in Fig. 9. Since all of the parameters are either in

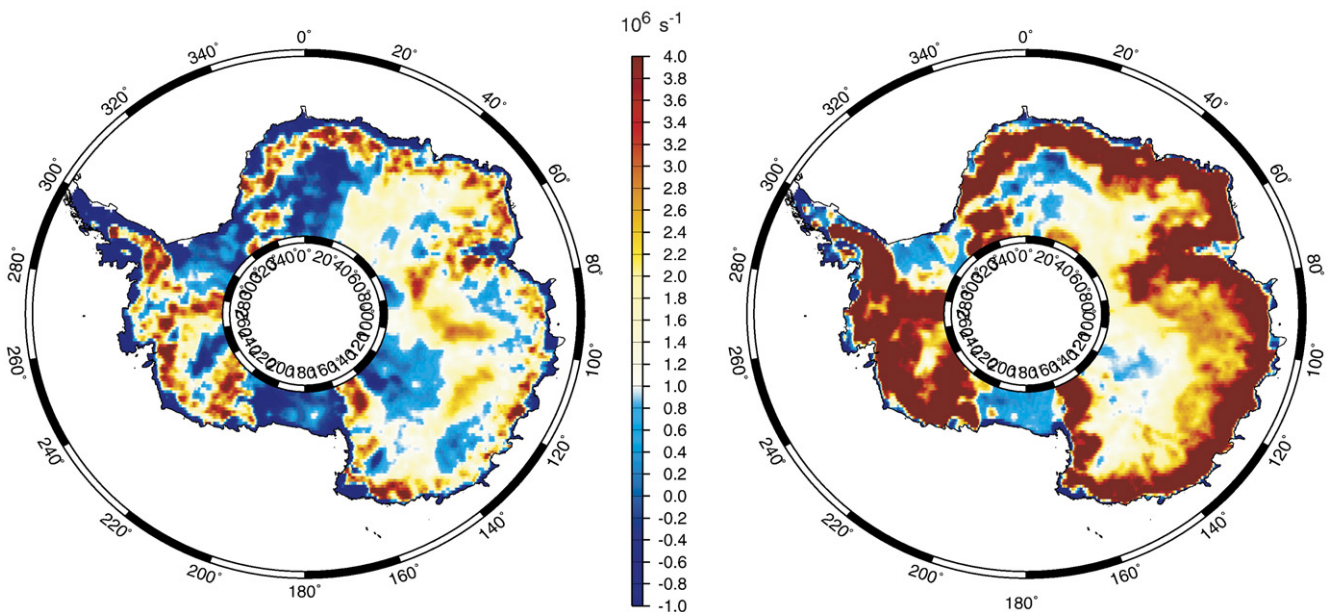


Fig. 4. Trailing edge slope map over the Antarctica plateau at S (left) and Ku band (right). Unit is  $10^6 \text{ Np s}^{-1}$ .

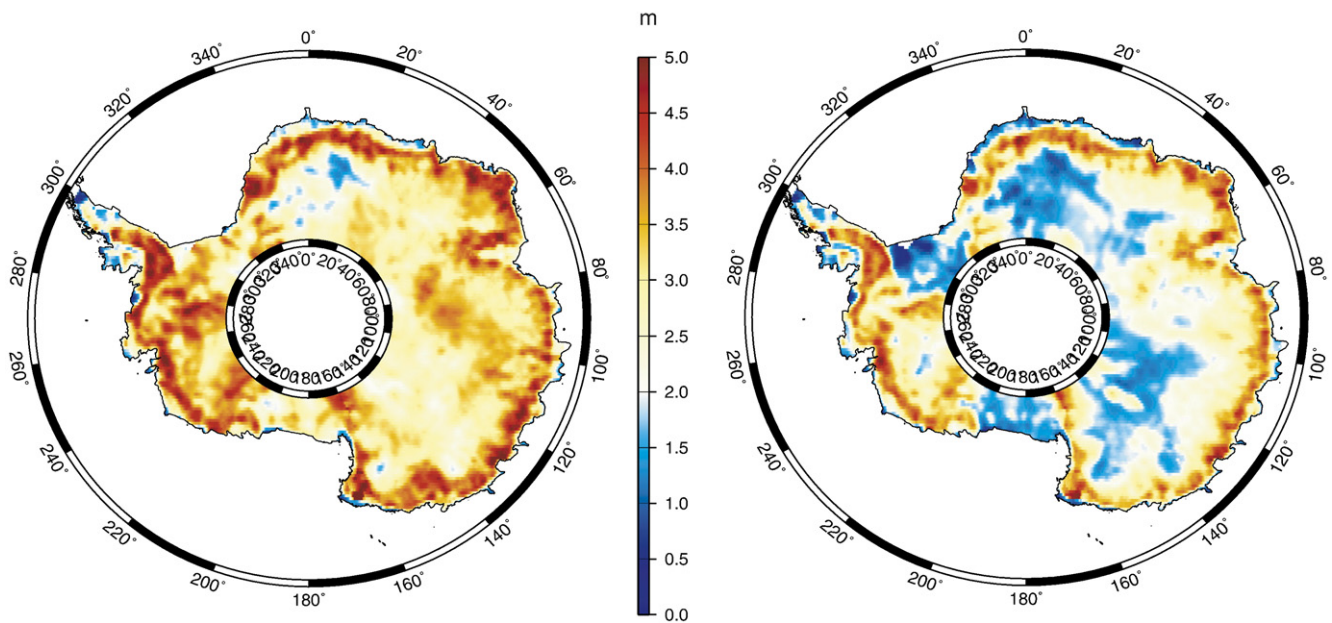


Fig. 5. Leading edge width map over the Antarctic continent at S (left) and Ku band (right). Unit is m.

or out of phase, only the date of the backscatter coefficient peak is mapped in Fig. 9. We clearly observe that the amplitude variations for each parameter are the greatest at the Antarctic borders decrease when we move towards the center of the continent, and increase again over the dome regions.

The main characteristics of the variations are: 1/ that the amplitudes are greater for the S than the Ku band, 2/ that the amplitudes and the phases vary over the ice-sheet, 3/ that the TeS and the LeW are in phase whereas the  $\sigma_0$  is out of phase. Finally 4/ another study based on along track measurements (Legrésy et al., 2006) shows that the altitude variations are in phase with  $\sigma_0$ , and that their amplitudes are about half of the LeW amplitude. All

these observations suggest that these seasonal variations are caused by a seasonal change in the snowpack properties which affects the two radar bands differently.

### 3. Evidence of the effect of surface roughness on the waveform characteristics

#### 3.1. Statistical observations

A statistical comparison is made for the four parameters averaged over 4 years. The Ku and S band  $\sigma_0$  values are well correlated with a correlation factor of 0.84 (Fig. 3). The comparison

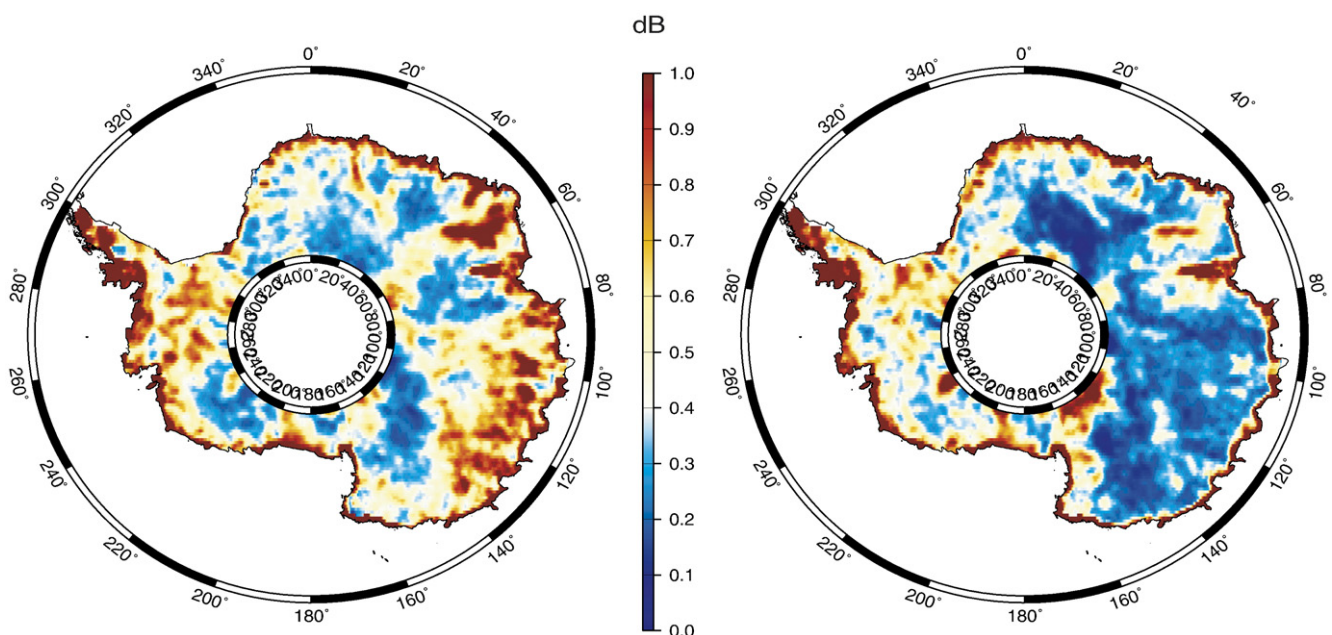


Fig. 6. Amplitude of the seasonal variations of the backscatter coefficient at S (left) and Ku bands (right). Unit is dB.

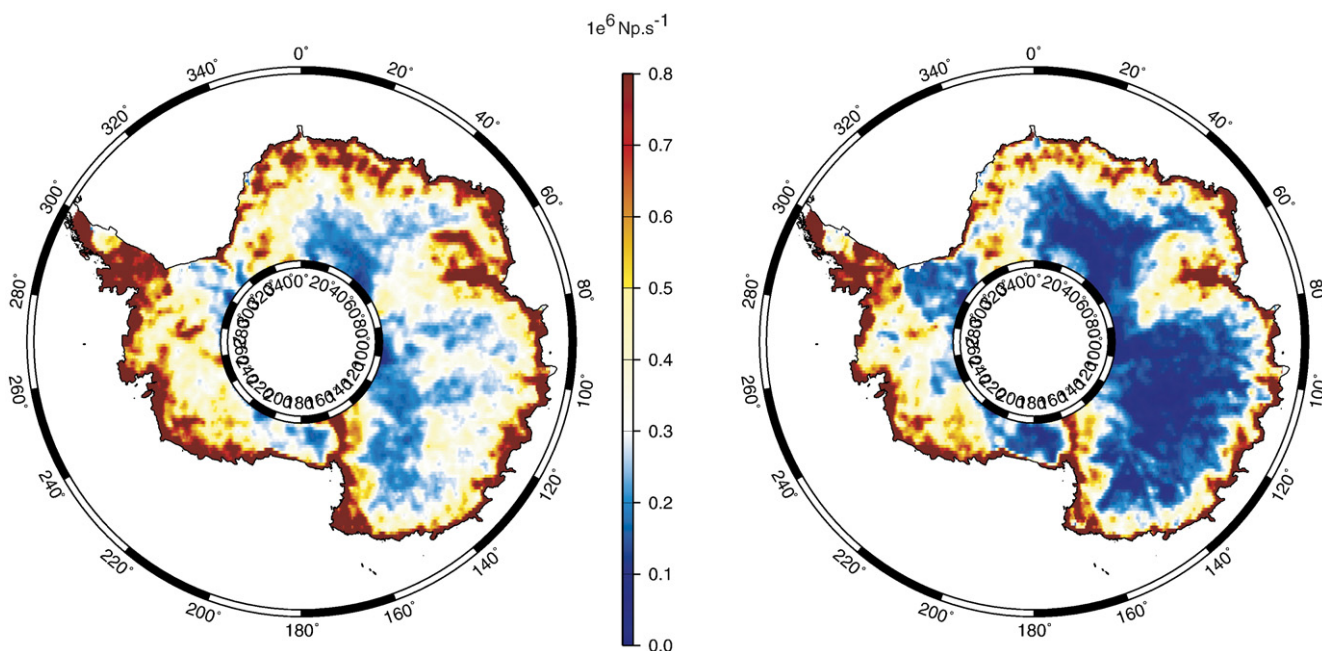


Fig. 7. Amplitude of the seasonal variations of the trailing edge slope at S (left) and Ku bands (right). Unit is  $10^6 \text{ Np s}^{-1}$ .

of TeS for the Ku ( $\text{TeS}_{\text{Ku}}$ ) and S bands ( $\text{TeS}_{\text{S}}$ ) also shows good spatial correlation (the correlation factor is 0.7), but their histograms are shifted.  $\text{TeS}_{\text{S}}$  is generally smaller than  $\text{TeS}_{\text{Ku}}$ , and around 10% of the Antarctic ice-cap exhibits negative values of  $\text{TeS}_{\text{S}}$  against 1.7% for  $\text{TeS}_{\text{Ku}}$ . Moreover, there is a clear anti-correlation between TeS values and  $\sigma_0$ ; low values of  $\sigma_0$  match well with high values of TeS. This waveform behaviour shows that altimetric waveforms are mostly related to one main property of the firm, which is the same for the Ku and S bands.

### 3.2. Trailing edge slope of the altimetric waveform

Here we consider the different geophysical parameters acting on the trailing edge slope behaviour of the waveform. These include the topography (the surface slope is called  $\theta_{\text{slope}}$ ), the snow surface small-scale roughness, the sub-surface characteristics and the extinction properties.

The topography impacts on the TeS and biases it toward greater values. Indeed a slope in topography contributes to shifting the first

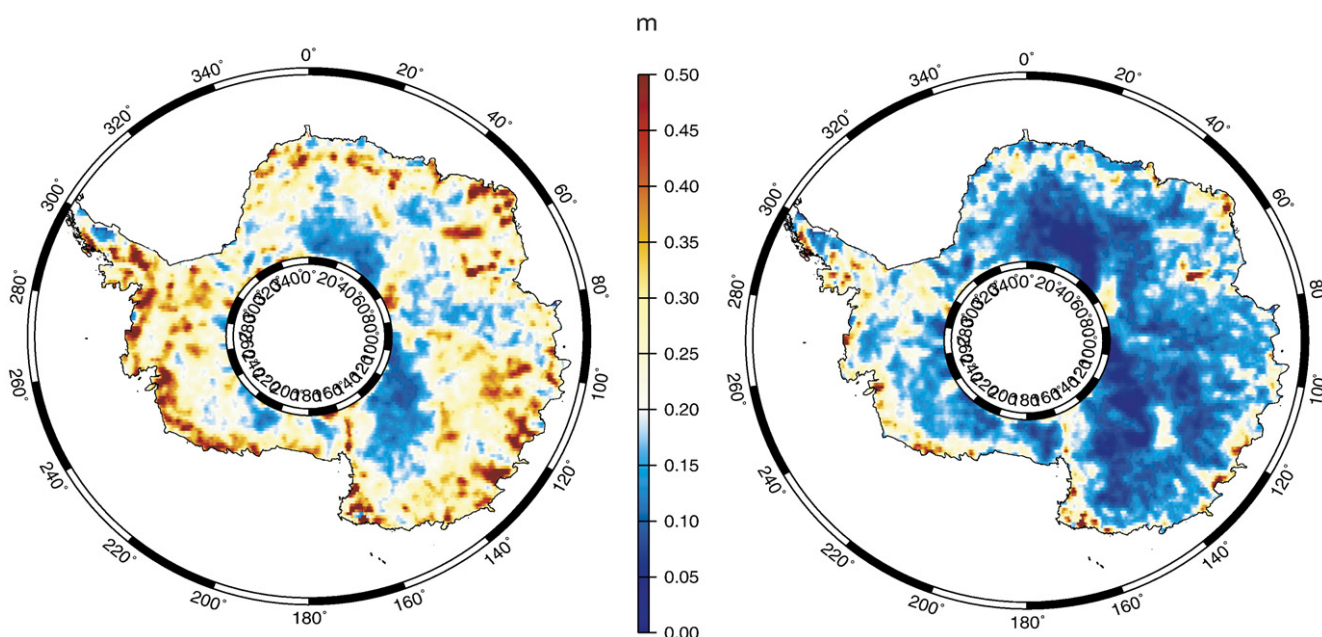


Fig. 8. Amplitude of the seasonal variations of the leading edge width at S (left) and Ku bands (right). Unit is m.

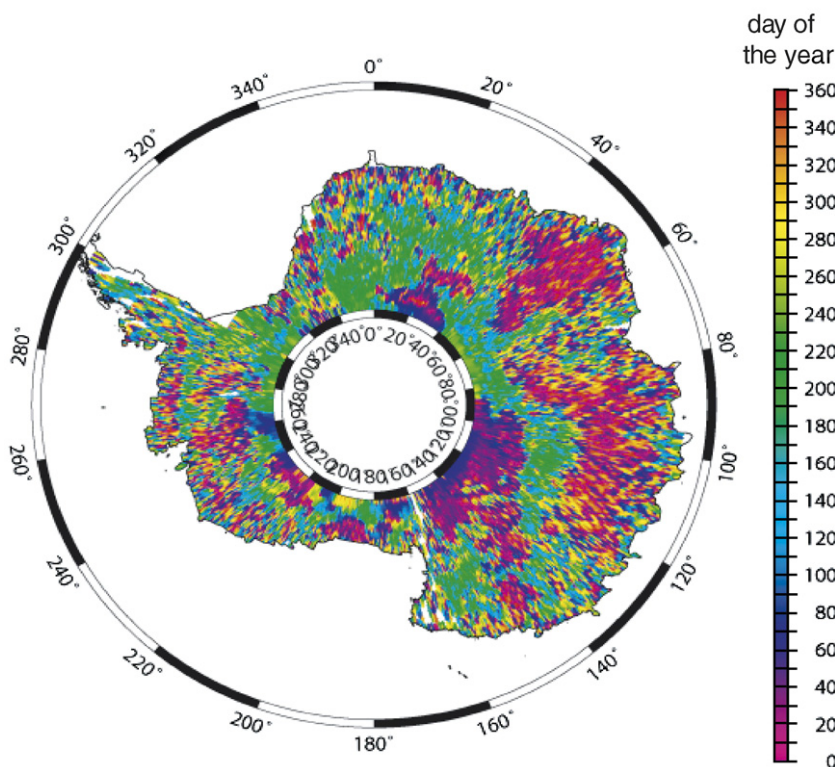


Fig. 9. Phase of the peak of maximum backscatter at Ku band given in day from January 1st. The phase maps for the leading edge width and the trailing edge slope are 6 months delayed.

point of impact off nadir, which leads to a decrease in the first radar echo because of the lower antenna gain off nadir. As a result the first echo is lowered compared to the later echoes, and TeS is higher.

The sub-surface signal also always contributes to increasing the trailing edge slope. The volume illuminated by the radar wave increases with time. As a result, the sub-surface signal back-scattered by the snow increases after the surface impact, creating an increase of the trailing edge slope. Thus, both topographic slope and the sub-surface signal have a positive effect on the trailing edge slope, and cannot be used to explain the observed negative values.

On the contrary the effect of small-scale roughness on the trailing edge slope is always negative. The radar wave reflected by a rough surface at nadir is the sum of a specular component and a scattered component. Smooth surfaces reflect more energy at the vertical incidence than rough surfaces. If this reflected component is the main component of the scattered signal, the energy backscattered by the surface presents a strong dependence with the incidence angle. The incidence angle is an increasing function of the time of observation. Therefore, the backscatter contribution of the surface decreases with the observation time. Thus, roughness effects always introduce a bias in the trailing edge slope toward negative values.

In summary, because of the presence of a specular component, waveforms acquired over smooth surfaces present high values of  $\sigma_0$  and low values of TeS. Since surfaces will always be considered smoother at lower frequencies, this behaviour is stronger and more common for the S band than the Ku band. Roughness effects can explain all of the observations made

previously at Ku and S bands. The roughness scale to be considered is then the scale that leads to the decrease of  $\sigma_0$  with  $\theta$  around  $0^\circ$ . The surface radiation pattern  $\sigma_0(\theta)$  is controlled by roughness parameters on the order of a fraction of a wavelength, that is, at the centimetre scale for the S and Ku bands (e.g. Ulaby et al., 1982). The effect of micro-scale roughness over ice-caps has also been pointed out by Oveisgharan and Zebker (2007) in SAR data, where they showed that a volume model can't explain the decrease of power observed with the angle of incidence.

Once corrected for the topographic bias, TeS is then a combination of opposing sub-surface signal and surface roughness effects. Positive values of the trailing edge slope show evidence of a strong sub-surface signal, whereas negative values reveal stronger surface roughness effects.

## 4. Waveform modelling

### 4.1. Background modelling

In the existing altimetric echo models, the radar surface return is based on the Brown model (1977), where the waveform is found through the convolution of the transmitted signal with the flat impulse response ( $P_{FS}$ ) and the point height probability ( $p_\chi$ ). The flat impulse response is related to the backscatter cross-section  $\sigma_0$  of the target, which in most cases is assumed to be constant over the range of incidence angles (for ENVISAT between  $0^\circ$  and  $0.6^\circ$  off-nadir). The dependence of  $\sigma_0$  with  $\theta$  is related to the roughness at the wavelength scale (Ulaby et al., 1982). Femenias et al. (1993) and Adams and Brown (1998)

apply a high frequency limit to describe this dependence, and consider a rough snow surface at the wavelength scale. As we have seen in the previous section (Section 3.2), the rough surface assumption is not true for lower radar frequencies.

Ridley and Partington (1988) modelled the half space beneath the surface with Rayleigh scatterers. They have shown that a major contribution to the signal comes from the volume scattering. Femenias et al. (1993) or Davis and Moore (1993) follow the same approach to model the volume contribution. This single scattering assumption overestimates the results, and some authors (e.g. Davis & Moore, 1993) add an empirical corrective factor that considers multiple scattering.

Legrésy and Rémy (1997) use a radiative transfer approach and consider both the layering and the volume scattering by combining their effects into an equivalent radar cross-section per unit of depth. This approach considers the same dependence on  $\theta$  for the two processes. Their model does not relate the backscatter cross-section to any geophysical properties of the snow. Adams and Brown (1998), have shown that the radiative transfer approach is equivalent to the Brown surface model, and define the volume contribution as a function of the average scattering properties of the sub-surface. Their model hence exhibits the same limitations as the model developed by Legrésy and Rémy (1997). They apply their model to a two layered medium. The application to a multiple layered medium has been made by Leushen et al. (2003) at low frequencies, and does not take into account the volume scattering.

This brief review highlights two main limitations when using the existing models for the S and Ku bands over the Antarctic ice-sheet: 1/ the backscattering properties of the target are poorly related to the geophysical properties of the snowpack, and 2/ the models empirically consider the dependence of  $\sigma_0$  with the incidence angle  $\theta$ , and so they poorly account for the small-scale roughness effects. For these two reasons, existing models are not well suited to exploit multiple frequency datasets. In this paper, we correct for these two limitations by adapting the Brown model (1977).

Modelling the altimeter signal in the frequency range 3–14 GHz acquired on a layered snow medium is not trivial, because the electromagnetic properties of the snow vary within this frequency range. For example, at frequencies above 10 GHz the dominant source of backscatter in the altimeter signal is due to scattering by snow grains. At higher frequencies, the signal is more sensitive to the reflections on the stratified medium due to the better penetration in the snow. GPR (Ground Penetrating Radar) profiles have been obtained at frequencies close to altimeter frequencies (Langley et al., 2007, submitted for publication) in order to determine sources of backscatter in the snow in the GHz range. These profiles provide good examples of the complexity of the radar signal.

#### 4.2. Impulse response of a layered media

The general form of the radar response  $P_r(t)$  on a medium of impulse response  $I(t)$  is given by:

$$P_r(t) = P_e(t) \otimes I(t) \quad (1)$$

where  $P_e(t)$  is the transmitted signal power, and  $\otimes$  denotes the convolution operator.

##### 4.2.1. The Brown surface model

The form of the impulse response of a rough surface is given by Brown (1977):

$$I(t) = P_{FS}(t) \otimes p_x(t) \quad (2)$$

where  $p_x(t)$  is the height probability function of the specular points at the surface and  $P_{FS}(t)$  is the flat surface impulse response. In the case of a vertical looking radar,  $P_{FS}$  is calculated by using the classical radar equation integrated over the illuminated surface:

$$P_{FS}(t) = \frac{\lambda^2}{(4\pi)^3} \int_S \frac{\delta\left(t - \frac{2r}{c}\right) \sigma_s^0(\theta) G^2(\theta)}{r^4} dS \quad (3)$$

where  $r$  is the range from the radar to the elementary surface  $dS$ ,  $\lambda$  is the radar wavelength,  $\sigma_s^0$  the backscatter cross-section of the target,  $\delta(t)$  the Dirac distribution, and  $G(\theta)$  is the antenna pattern. The term  $t' = \frac{2r}{c}$  can be rewritten to depend only on  $\theta$  by considering the problem geometry (Fig. 10):

$$t'(z = 0, \theta) = \frac{2H}{c} \frac{1}{\cos(\theta)} \quad (4)$$

where  $H$  is the satellite height.

$G(\theta)$  is given by Legrésy et al. (2005) as:

$$G(\theta) = G_0 e^{-\alpha \theta_{\text{slope}}^2 - (g_0 - \beta \theta_{\text{slope}}) \gamma \cdot \left(\frac{2H}{c} \left[1 - \frac{1}{\cos\theta}\right]\right)} \quad (5)$$

Where  $G_0$  is the antenna gain,  $g_0$ ,  $\alpha$  and  $\beta$  are positive antenna parameters,  $\theta_{\text{slope}}$  the topography slope and  $\gamma$  a parameter related to the surface curvature following the notations in Legrésy et al. (2005), where corresponding ENVISAT values of all these parameters can be found.

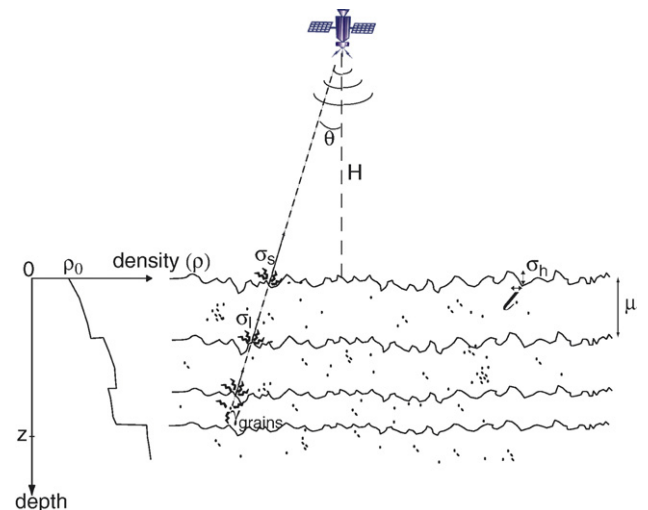


Fig. 10. Scheme of the radar geometry and parameters definition.

The loss in  $r^{-4}$  (Eq. (3)) can be considered to be almost constant within the illuminated surface, and then can be moved out the integral. Finally, the integral in Eq. (3) is reduced to a function of the angle  $\theta$  only.

#### 4.2.2. Sub-surface model

##### 4.2.2.1. Application of the Brown model to a layered media.

The Eq. (3) is well adapted for computing the radar response to a radially distributed medium. However, this is not our case, since snowpacks are layered media. Hence, in the following we separate the vertical from the horizontal axes to express the time of integration  $t' = \frac{2x}{c}$  in the Eq. (3) as a function of the horizontal ( $\theta$ ) and the vertical directions ( $z$ ). Since the altimetric incidence angles are small, we assume that any point  $P(z, \theta)$  of the snowpack is reached at a time  $t'$ , where  $\theta$  and  $z$  can be separated, so that:

$$t'(z, \theta) = t_v(z) + \frac{2H}{c \cdot \cos(\theta)} \quad (6)$$

The two-way vertical travel time in the snow  $t_v$  is related to the depth through a vertical permittivity profile of the snow  $\epsilon'(z)$ :

$$t_v(z) = 2 \int_0^z \sqrt{\frac{\epsilon'(z') dz'}{c}} \quad (7)$$

The Dirac function  $\delta$  in Eq. (3) can then be rewritten by separating the variables  $\theta$  and  $z$ :

$$\delta(t - t'(z, \theta)) = \delta(t - t_v(z)) \otimes \delta(t - t'(z = 0, \theta)) \quad (8)$$

The small angle approximation allows us to consider that all of the paths in the snow are strictly along the  $z$  axis. Therefore the off-nadir delay is not different from that at  $\theta=0$  (the error is of  $O(-4)$ ). This means that the  $P_{FS}$  function for a buried interface situated at depth  $z$  has the same expression as the  $P_{FS}$  function of the surface but different backscattering properties (both amplitude and variations with  $\theta$ ), which are attenuated by the above medium, and shifted in time by  $t_v(z)$ . Thus we can easily express the sub-surface model through the convolution of the Flat surface impulse response combined with a vertical distribution of the scattering properties of the medium, as shown by Adams and Brown (1998).

4.2.2.2. Sub-surface impulse response. The radar echo returned by a snowpack is the result of two different physical processes which depend on the frequency (Wiesman & Matzler, 1999):

- surface echoes are related to the snow density heterogeneity at the layer interfaces  $\sigma_1^0(z, \theta)$ , and depend on  $\theta$ .
- scattering by small snow grains:  $\gamma_{\text{grains}}(z)$ , which is independent of  $\theta$ . This scattering is expressed per unit of volume  $dV = dS \cdot dz$ .

Following Adams and Brown (1998), we express the sub-surface model by the convolution of the Brown model with a

distribution of the scattering sources  $p_v(z)$  function of the depth (or the vertical travel time in the snow  $t_v(z)$ ). The expression of  $\sigma_s^0$  in Eq. (3) changes for the cases of grain scattering or for the interfaces. The expression of  $p_v(t_v)$  depends on the vertical distributions of the scatterer sources.

The “flat volume” impulse response  $P_{FV}$  is then given by:

$$P_{FV}(t) = P_l(t) \otimes p_{vl}(t_v) + P_g(t) \otimes p_{vg}(t_v) \quad (9)$$

Where  $P_l$  and  $P_g$  are respectively the flat impulse response for the layers and the grains, and  $p_{vl}$  and  $p_{vg}$  are the vertical scattering distributions for the layers and the grains.  $p_{vl}$  has a discrete distribution with zero values, except at the times  $t_v$  corresponding to the depth  $z$  of the density discontinuities.  $p_{vg}$  is a continuous distribution depending on the scattering and extinction by the snow grains. Hence, the “flat volume” impulse response of the Eq. (9) is now given by:

$$P_{FV}(t) = \frac{1}{(4\pi)^3 H^4} [P_{\text{layers}} + P_{\text{grains}}]$$

$$P_{\text{layers}}(t) = \sum_{n=1}^N \lambda_n^2 \cdot A(z_n) \cdot \delta(t - t_v(z = z_n)) \otimes \int_S \delta(t - t'(z = 0, \theta)) \sigma_1^0(z = z_n, \theta) G^2(\theta) dS \quad (10)$$

$$P_{\text{grains}}(t) = \int_z \lambda^2(z) \cdot A(z) \cdot \delta(t - t_v(z)) \gamma_{\text{grains}}(z) dz \otimes \int_S \delta(t - t'(z = 0, \theta)) G^2(\theta) dS$$

Where  $A(z)$  is the extinction at the depth  $z$ ,  $N$  is the number of internal layers,  $\lambda_n$  is the radar wavelength at the depth of the layer  $n$ ,  $z_n$ . Practically,  $dz$  is calculated for each time  $t_v$  in terms of the dielectric properties of the medium. The different scattering properties of the sources are developed in the following, where we will focus on adding the small-scale roughness contribution, and relating the scattering properties of the sources to their geophysical properties.

#### 4.3. Surface scattering properties

The surface backscattering coefficient is related to the surface roughness at the scale of the radar wavelength (Ulaby et al., 1982). Its amplitude is proportional to the dielectric constant of the surface and its angular pattern is governed by the surface roughness. The two scales of roughness that are taken into account here are:

- 1/ Large scale, namely the sastruggi scale (50 cm over 10 m). Its effect on the shape of the waveform is classically modelled by the convolution with  $p_\gamma$ . Adams and Brown (1998) have simulated the effect of sastruggi scale roughness on the altimeter signal. The effect on  $\sigma_0$  is taken into account by a multiplicative factor  $\alpha$  ( $0 < \alpha < 1$ ). This factor can also be understood as a tuning factor between the sub-surface and surface model, as presented by Newkirk and Brown (1996).

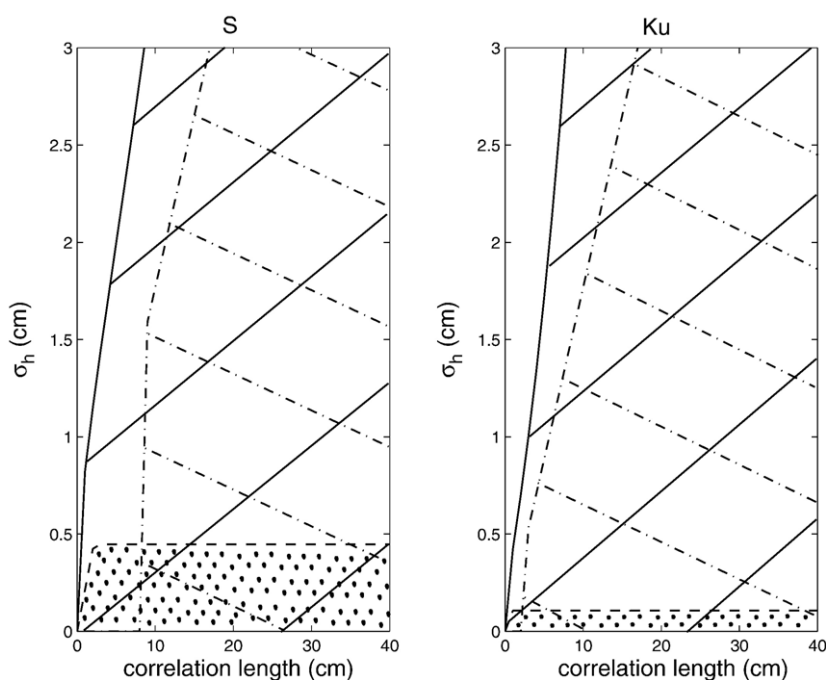


Fig. 11. Domain of validity of the Small Perturbation Model (points), Physical Optic (dashed stripes) and Integral Equation Method (plain stripes) for S (left) and Ku (right) waves.

2/ Small-scale roughness (5 mm over 10 cm). This scale results from the combination of precipitation, wind and grain characteristics at the surface. Since these roughness characteristics are of the same order as the altimeter wavelengths, the small-scale surface roughness directly influences the surface radiation pattern.

The small-scale snow surface roughness is described statistically by two parameters.  $\sigma_h$  is the standard deviation of the height distribution of the scatterers, which is assumed to be Gaussian.  $l$  is the correlation length of the surface. Roughness measurements over snow surfaces at centimetre scales have rarely been carried out. Measurements undertaken on other surfaces such as ice (Rees & Arnold, 2006) or agricultural soils (Zribi et al., 2000; Jackson et al., 1997) provide an idea of the range of variations of these parameters.  $\sigma_h$  ranges from 4 mm to 3 cm, and  $l$  ranges from 3 cm to 20 cm. These figures are coherent with first promising measurements obtained on snow surfaces (Lacroix et al., submitted for publication).

The interaction between the surface and the incident wave can be modelled analytically. Beckmann and Spizzichino (1987) or Fung et al. (1992) investigated the domain of validity of different analytical methods: the Physical Optic (PO) approximation, the Small Perturbation Method (SPM), or the Integral Equation Method (IEM) (Fung, 1994). The IEM method provides the greatest application domain in the range between Ku and S bands (Fig. 11). Due to the lack of knowledge on the exact snow surface roughness parameters we will use the IEM method in the following analysis.

#### 4.4. Scattering properties of the internal layers

As for the air/snow interface, scattering at each internal layer depends on the dielectric contrast and the different scales of roughness. The internal roughness characteristics are assumed to be the same as the air/snow surface. However, because of the decrease of the radar wavelength in the snow, the internal layer radiation pattern  $\sigma_1^0(\theta)$  is different from the surface and appears relatively rougher. Thus,  $\sigma_1^0(\theta)$  is less sensitive to the variations of  $\theta$  and the amplitude of the backscatter is less important.

#### 4.5. Volume scattering

Snow grains play a role in the scattering, and thus the extinction of the signal, depending on the size of the scatterers ( $\Phi_g$ ) and the radar frequency  $f_0$ . The Rayleigh scattering approximation for small particles seems to overestimate the amplitude of the scattered field, by neglecting multiple scattering. Mätzler (1998) proposes to apply a modified Born approximation to granular media with strong dielectric fluctuations. Applying this method to media consisting of small rounded grains of ice ( $\epsilon'_i=3.15$ ) embedded in the air, with a volume fraction of  $v = \frac{\rho}{\rho_i}$  ( $\rho$  the snow density,  $\rho_i$  the ice density), corresponds to the Rayleigh approximation with a corrective factor. The corrective factor is related to the correlation length  $p_c$  of the media, as seen in Mätzler (1998).

$$\gamma_{\text{grains}} = \frac{3 p_c^3 k_0^4}{32} \cdot v \cdot (1 - v) \cdot (\epsilon'_i - 1)^2 \cdot K ds^2 \quad (11)$$

$$p_c = \frac{4 \cdot \Phi_g}{3} \cdot (1 - \nu) \quad (12)$$

$$K_{ds}^2 = \left| \frac{2 \cdot \epsilon' - 1}{2 \cdot \epsilon' + \epsilon'_i} \right|^2 \quad (13)$$

#### 4.6. Vertical distributions of the snow parameters

In this subsection, we define the vertical profiles of the different geophysical snow parameters used by the model. The density profiles in the snowpack are variable over the Antarctic ice-cap (Goodwin, 1988; Frezzotti et al., 2005; Gerland et al., 1999). For simplicity, we take the same density profile for all simulations, with a variation in the first 10 m given as:

$$\rho(z) = \rho_0 + p \cdot z + c_2 \cdot z^2 + c_3 \cdot z^3 \quad (14)$$

The coefficients  $c_2$  and  $c_3$  are constant values taken from the Talos Dome density profile (Frezzotti et al., 2005). The surface density  $\rho_0$  is an input parameter of the model, and the parameter  $p$  is calculated as a function of  $\rho_0$ , so that the density at the depth below the surface  $z=10$  m is the density measured at the Talos Dome.

Density heterogeneities  $\Delta_\rho$  are superimposed on this general trend in  $\rho$  (Fig. 10), which originate from echoes from the layering. Mean  $\Delta_\rho$  measurements have been undertaken at a fine resolution from 2 m snow pits, and range from  $0.02 \text{ g cm}^{-3}$  to  $0.1 \text{ g cm}^{-3}$  (Jezek et al., 1988; West et al., 1996). Density observations (Gow, 1968) in snow cores show that the density fluctuations at centimetre scales decrease with increasing density. As such, we assume that the mean density transition follows the density profile and vanishes as the snow becomes ice:

$$\Delta_\rho(z) = \delta_\rho \frac{\rho_i - \rho(z)}{\rho_i - \rho_0} \quad (15)$$

$\delta_\rho$  is the mean density transition at the surface. Altimeters have a large vertical resolution compared to the snow layer thicknesses, so the intensity of the internal layer reflections is described by both the number of layers per radar bin (or the mean layer thickness) and the mean density transition between layers  $\Delta_\rho$ . Since both the layer thicknesses and  $\Delta_\rho$  have the same impact on the signal intensity, we have chosen to allow a variable layer thickness and to fix  $\delta_\rho$  to  $0.05 \text{ g cm}^{-3}$ . The layer thicknesses are assumed to decrease with increasing density, due to the snow compaction, so the layer thicknesses actually refer to a water equivalent thickness (or an accumulation rate  $\mu$ ).

The complex relative dielectric constant of snow ( $\epsilon' + i \cdot \epsilon''$ ) has been measured as a function of the snow density  $\rho$  expressed in  $\text{g cm}^{-3}$  (Tiuri et al., 1984):

$$\epsilon' = 1 + 1.7 \cdot \rho + 0.7 \cdot \rho^2 \quad (16)$$

$$\epsilon'' = \epsilon_i'' \cdot (0.52\rho + 0.62\rho^2) \quad (17)$$

The temperature,  $T$ , and frequency,  $f$ , dependence of  $\epsilon_i''$ , has been studied by Matsuoka et al. (1996), at low

temperature 190–265 K for radar frequencies between 5 and 39 GHz:

$$\epsilon_i'' = \frac{A(T)}{f} + B(T) \cdot f^{C(T)} \quad (18)$$

where  $A$ ,  $B$  and  $C$  are functions of the temperature.

Finally, we assume that the temperature and the snow grain size are constant over the depth profile. The snow grain growth rate is neglected here, since the volume scattering only affects the Ku band signal. Thus, the snow grain size chosen here is an equivalent snow grain size over the entire snow thickness, as detected by the Ku wave. We will also see later that only the Ku band signal is sensitive to changes in temperature, so that the constant temperature profile does not limit the comparison of the two radar signals.

#### 4.7. Extinction

The power extinction in a layered snowpack is given by both the extinction due to the medium composed of snow grains and the scattering due to the layer interfaces:

$$A(z) = \exp^{-2 \cdot \left( \int_0^z k_e dz \right)} \cdot \prod_{n=1}^N T_n^2 \quad (19)$$

where  $T_n$  is the transmittivity of the layer  $n$ . The extinction coefficient  $k_e$  for a low dense granular medium consisting of particles of ice surrounded by air is given by the sum of the absorption  $k_a$  and the scattering  $\gamma_{\text{grains}}$  coefficients following Mätzler (1998):

$$k_e = \nu \cdot k_0 \cdot \epsilon_i'' \cdot K_{ds}^2 + \gamma_{\text{grains}} \quad (20)$$

where  $\epsilon_i = \epsilon'_i + i \cdot \epsilon_i''$  is the relative permittivity of ice.

## 5. Results of the simulations

### 5.1. Comparison with observations

The model developed here is a derivation of the Brown model, where the scattering properties of the snowpack are not empirical but related to the properties of the snow and the frequency of the incident wave. Validating this model is not easy because of the lack of in situ data on snow properties over the ice-sheets. So, we first show that the model can reproduce waveforms simultaneously at S and Ku bands and secondly we test the sensitivity of the model to snow properties, using two locations on the plateau: Lake Vostok and Dronning Maud Land. These locations are chosen because the slope in topography is small and so has a minor impact on the waveforms. In regions with a stronger slope, the waveform parameters must first be corrected for the topographic effect, before fitting the model.

We first simulate the altimetric waveforms for a range of varying relevant input parameters in order to analyse their effects on the signal. The range of variation of these parameters is taken from in situ observations (Table 2). The input steps are

Table 2  
Range of variation of the snow parameters over the Antarctic ice-sheet

Parameter	Notation (units)	Min value	Max value	Step	References
Surface density	$\rho_0$ ( $\text{g cm}^{-3}$ )	0.2	0.5	0.02	Goodwin et al. (1988)
Accumulation rate	$\mu$ ( $\text{kg m}^{-2} \text{y}^{-1}$ )	0	2000	$\frac{1}{\mu}$ constant	Vaughan et al. (1999)
Snow grain size	$\Phi_g$ (mm)	0.1	1	0.1	Surdyk and Fily (1993)
Surface rms height	$\sigma_h$ (mm)	1	20	1	Lacroix et al. (submitted for publication)
Correlation length	$l$ (cm)	4	50	2	Lacroix et al. (submitted for publication)
Snow temperature	$T$ (K)	190	260	10	King and Turner (1987)

chosen using an iterative sensitivity study of the model outputs. The model is then adjusted to the real waveforms by fitting the 6 model parameters ( $\sigma_h$ ,  $l$ ,  $\Phi_g$ ,  $\mu$ ,  $\rho_0$ ,  $\alpha$ ) using a least square method over the three waveform parameters (LeW, Bs, TeS) at each band. The precision of the inversion is calculated by adding 10% noise to the input parameters over 100 runs. The inverted waveforms are chosen from parameters that are characteristic of the mean waveform parameters for the area.

The Vostok lake area is characterized by slopes of less than  $1 \text{ m km}^{-1}$ . The accumulation rate is very low, around  $30 \text{ kg m}^{-2} \text{ yr}^{-1}$  (Vaughan et al., 1999). The shallow snow grains are large, because of the low accumulation rate that creates a high growth rate. The annual mean temperature is around 220 K. The model fit reproduces the waveforms very well (Fig. 12). The snow parameters estimated with this fit are a good first approximation of the real snowpack properties (Table 3). The parameter  $\mu$  is around  $80 \text{ kg m}^{-2}$  with high variability, indicating that the inversion is not very sensitive to this parameter. The grain size is

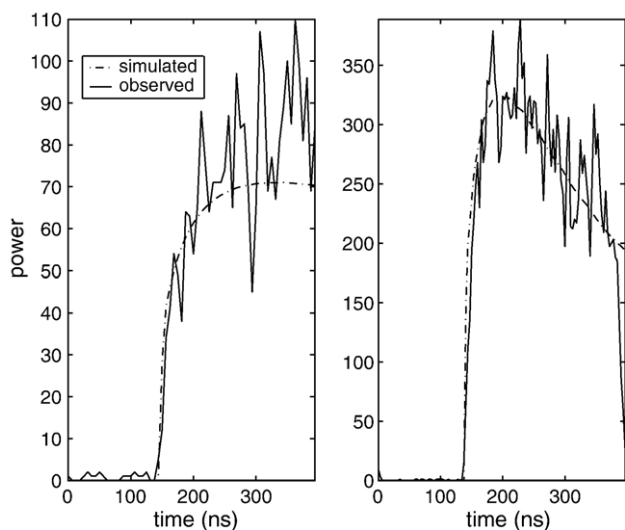


Fig. 12. Waveform observed (solid) and modelled (dashed) over the Vostok lake (lat=104.126°, lon=-76.574) at S (left) and Ku band (right). The parameters found by the inversion are written in the Table 3.

Table 3  
Snow parameters inversion at 2 locations (Vos=Vostok, Mau=Dronning Maud Land) based on the fit on individual waveforms represented in the Figs. 12 and 13

Location (lon, lat)	$\rho_0$ ( $\text{g cm}^{-3}$ )	$\mu$ ( $\text{kg/m}^2$ )	$\Phi_g$ (mm)	$\sigma_h$ (mm)	$l$ (cm)
Vos (104.13, -76.57)	$0.24 \pm 0.03$	$80 \pm 70$	$0.9 \pm 0.07$	$3.9 \pm 0.3$	$14 \pm 3.6$
Mau (9.83, -74.96)	$0.34 \pm 0.05$	$422 \pm 339$	$0.8 \pm 0.17$	$4.8 \pm 0.5$	$33.5 \pm 4.9$

The error range is found by considering a signal to noise ratio on the waveforms of 10%.

relatively large (0.9 mm), which indicates that the growth rate is important. In this region, the high trailing edge slope indicates that the sub-surface signal is more important than the surface signal, given by the model through a rough surface ( $\sigma_h=4 \text{ mm}$ ,  $l=14 \text{ cm}$ ).

The model is also fitted to the Dronning Maud Land waveforms (Fig. 13), where low trailing edge slopes and high backscatter coefficients have previously been observed. Based on a regional atmospheric climate model, Van den Broeke and Van Lipzig (2003) reported strong geostrophic winds ( $>10 \text{ m s}^{-1}$ ) in July, inducing an important sublimation and/or erosion rate. In winter, the precipitation rate is very low. These two factors contribute to low accumulation rate and a smooth surface. Turner et al. (1999) reported an area of negative mass balance, extending from the Ronne Ice Shelf northwards up to the coast of Dronning Maud Land, due to an unusual evaporation sublimation during the summer. Hence, this region is subjected to a constant net loss in summer and in winter. We assume here that the net loss and the constant wind and sublimation favour the smoothing and the compaction of the surface. The roughness parameters found here are in agreement with these observations (Table 3). Indeed surfaces are found to be very flat ( $\sigma_h=4.8 \text{ mm}$ ,  $l=34 \text{ cm}$ ) and the surface density is relatively high. The low trailing edge slope and the

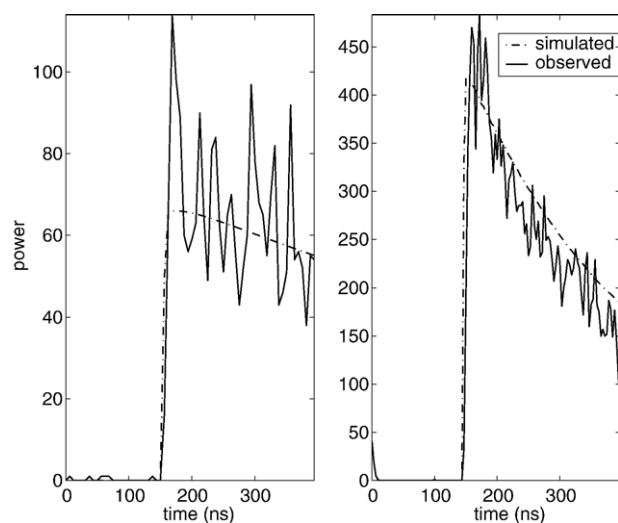


Fig. 13. Waveform observed (solid) and modelled (dashed) on Dronning Maud Land at the position (lat=9.838°, lon=-74.954) at S (left) and Ku band (right). The parameters found by the inversion are written in the Table 3.

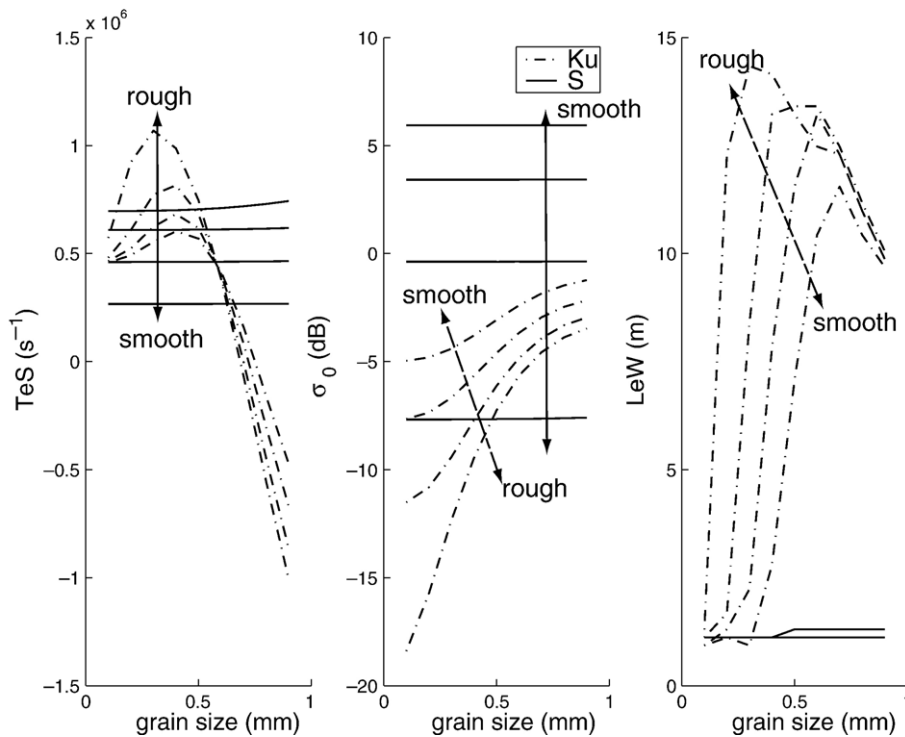


Fig. 14. Effects of the snow grain size on the waveform parameters (from left to right: the trailing edge slope, the backscatter coefficient, the leading edge width), at Ku (dashed) and S band (solid).

high backscatter coefficient are correctly interpreted by the model through the smooth surface.

This inversion shows the model capacity to simulate the dual-frequency signal. However, the waveforms are highly

sensitive to undulations in the topography at large scales, that create variations in the LeW. The model fit, based only on the waveform parameters does not always lead to a reliable inversion.

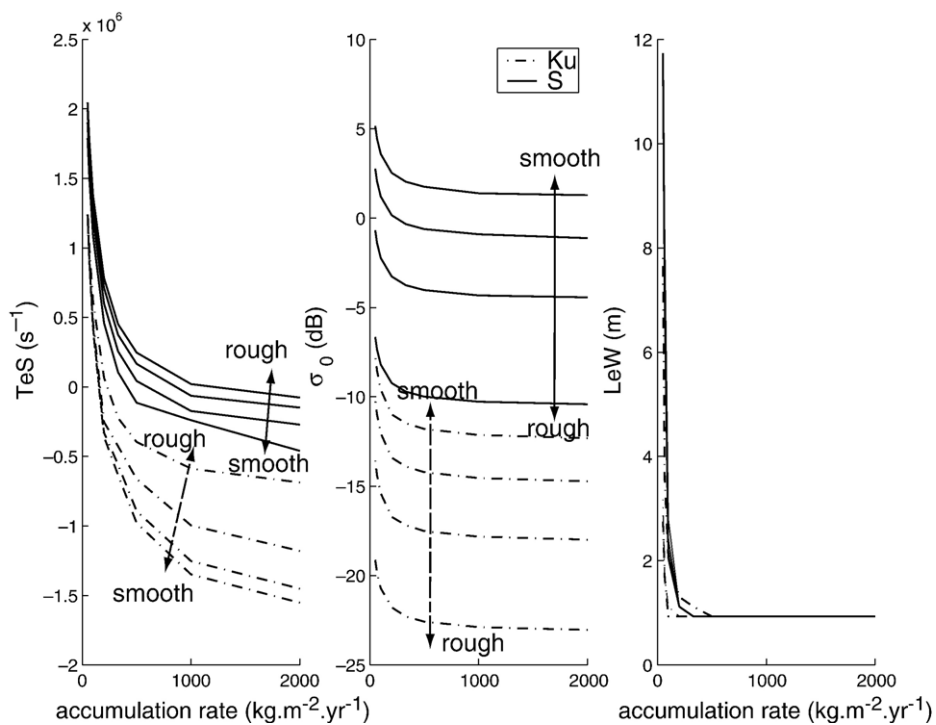


Fig. 15. Effects of the mean layer thickness on the waveform parameters (from left to right: the trailing edge slope, the backscatter coefficient, the leading edge width), at Ku (dashed) and S band (solid).

## 5.2. Simultaneous snow properties dependence

### 5.2.1. Analysis

The effects of different snow properties on the altimeter parameters are now investigated. The waveform parameters are governed by the combination of surface roughness effects and sub-surface signals (Figs. 14 and 15). For a smooth surface, an increase in the sub-surface contribution does not play a major role in the TeS, because the strong surface effect masks the sub-surface effects. However, for a rough surface the relative importance of the sub-surface contribution is greater, leading to a higher TeS. Therefore, the effect of snow grain is of primary importance at the Ku band for a rough surface (Fig. 14). We notice that the Ku and S signals respond differently to snow grain size. At S band, the effect is almost negligible. So a comparison of the two signals can be useful for estimating snow grain size.

The simulations show the importance of the surface roughness effects at the S and Ku bands in relation with the layering echoes (Fig. 15). Layering has a surface effect, and thus a change in roughness directly impacts on the signal from the layers. Also, the layer size directly impacts on the number of dielectric discontinuities in the snowpack; therefore smaller

layers create a greater signal. Our modelling shows that the radar altimeter is very sensitive to the accumulation rate at low accumulation rates. This underscores the capacity of the radar altimeters for retrieving the accumulation rate in Antarctica on the inland plateau, where the accumulation rate is low.

### 5.2.2. Glaciological implications

Based on the previous analysis, the regions of the Antarctic ice-sheet where S or Ku waveforms present high  $\sigma_0$  and low TeS values correspond to an important surface signal (smooth surfaces), and a smaller sub-surface signal compared to the surface. These regions of low trailing edge slopes and high backscatter coefficients are situated in Queen Maud Land, Marie Byrd Land, the central East Antarctica plateau, the western borders of the Ross Ice-Shelf, and on the ice-shelves. The main signal affecting the radar return in both bands in these regions is therefore the surface signal.

These regions where the surface signal dominates are interesting for ice-sheet mass-balance studies. In these regions the sensitivity of the Ku signal to the sub-surface effects is negligible. This is also enhanced by the observation of the leading edge width in these regions (Fig. 5), which exhibits small values, synonymous with small sub-surface contribution. Thus, the

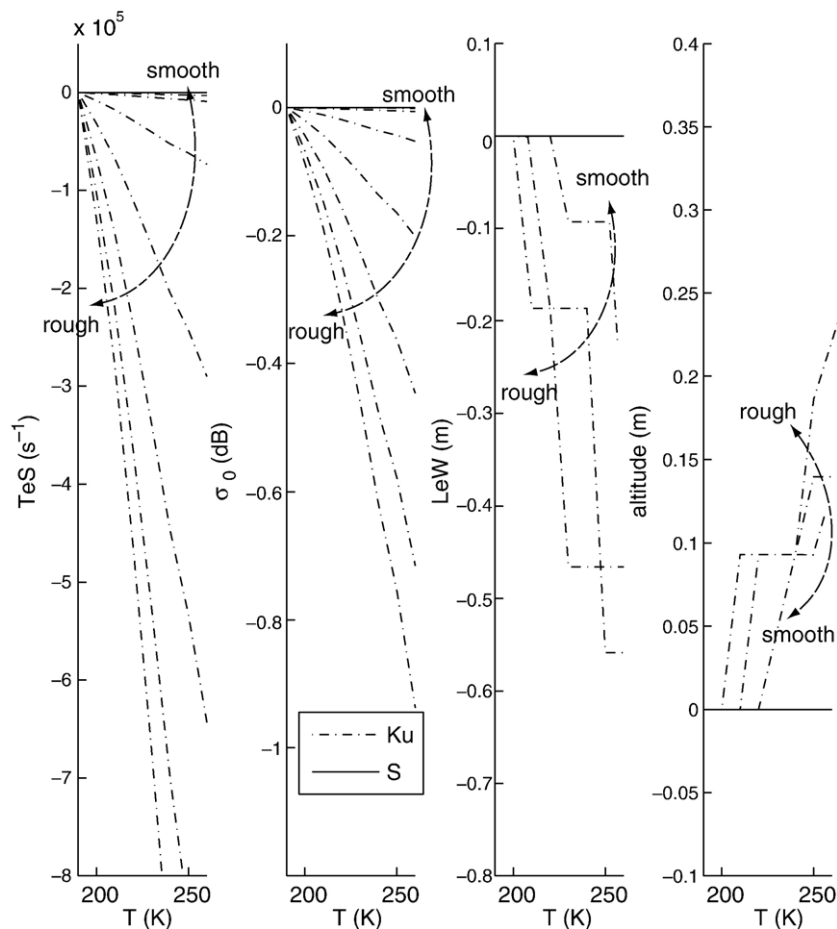


Fig. 16. Effects of the temperature on the variation of the waveform parameters (from left to right: the trailing edge slope, the backscatter coefficient, the leading edge width, the altitude), at Ku (dashed) and S band (solid).

retracked altitude is completely correlated to the surface elevation, and these regions can be used as “test” areas for mass-balance studies.

### 6. Seasonal variations of the altimetric signal

As seen in Section 2.2, all of the waveform parameters are affected by seasonal variations. The LeW and the TeS decrease simultaneously, whereas  $\sigma_0$  increases (cf Fig. 2). The phase of this cycle varies depending on the locations. In order to explain this behaviour, we compare two different hypotheses: 1/ that the temperature cycle creates a variation of the wave penetration properties, and 2/ that the snowpack compacts due to the temperature cycle and the heat-vapour transfer (Li Jun & Zwally, 2002, 2004).

#### 6.1. Temperature cycle

The temperature modifies the conductivity of the snow medium (Matsuoka et al., 1996). As the temperature increases, the dielectrical loss in the snow becomes higher, and the wave penetration decreases. So, variations in temperature are thought to impact more on the altimeter waveforms when the volume signal is high compared to the surface signal.

We have simulated the waveform parameters for varying temperatures and for different roughness when the volume signal is important, that is, when the snow grains are large and the layer thickness is small (Fig. 16). The amplitude of the temperature variations between summer and winter can reach up to 50°, but still remains below freezing on the Antarctica plateau, which keeps the snow dry.

The model shows that the Ku band is sensitive to temperature, while the S band is not. A temperature increase causes the values of the Ku band waveform parameters to fall, including the backscatter coefficient. This can be explained by the increase of the snow extinction as the temperature increases.

However, temperature variations cannot explain the seasonal variations observed in the altimetric signal for 3 main reasons: 1/ The S signal is not sensitive to temperature variations. 2/ A temperature increase creates correlated variations of all of the waveform parameters, and does not explain the anti-correlation between the backscattering coefficient and the LeW and TeS (Fig. 2). 3/ The temperature variations only explain the maximum of the parameters when the temperature is the lowest, i.e. in winter.

In summary, the temperature hypothesis is rejected as the main cause of the seasonal signal. However, the model shows that the temperature cycle can explain large variations of the waveform parameters in the Ku band, in particular the altitude

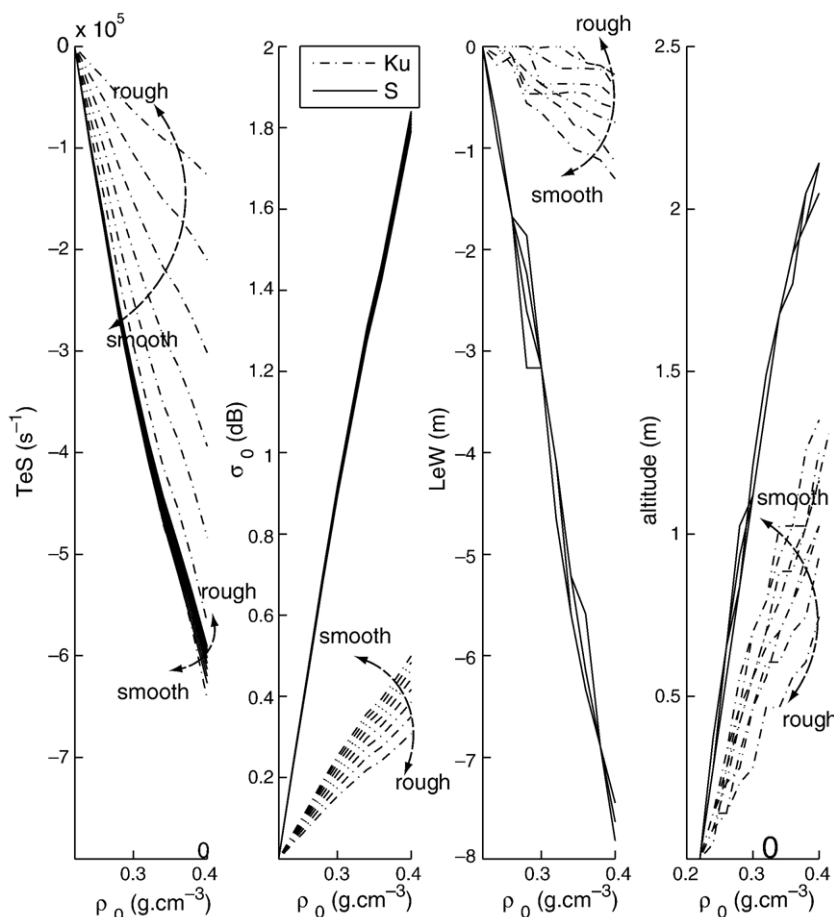


Fig. 17. Effects of the surface density on the variation of the waveform parameters (from left to right: the trailing edge slope, the backscatter coefficient, the leading edge width, the altitude), at Ku (dashed) and S band (solid).

(up to 25 cm for a temperature variation of 40 K). The temperature variation is not the main effect on this signal, but must be taken into account. The temperature effect could also explain the phase delay between the S and Ku bands observed in Fig. 2, because of the difference in sensitivity of this parameter between the two radar bands.

## 6.2. Snowpack compaction

Li Jun and Zwally (2002, 2004) showed that compaction rate of the snowpack depends on the season of the year. They first modelled snow densification by forcing the air-temperature cycle with a constant accumulation rate during the year. They found that only high accumulation rates produce high compaction rates, and that the strong amplitudes observed in the retrieved altitude in low accumulation areas cannot be explained by the temperature process. They improved their model by adding a heat-vapour transfer component, that creates a densification of the snow layers when they are buried (Li Jun & Zwally, 2004). This mechanism is more efficient at low accumulation rates and can produce variations in snow density in the first 2 m of greater than  $100 \text{ kg m}^{-3}$ . Nevertheless, a process of accumulation and compaction cannot explain variations in height greater than the accumulation rate, nor the amplitude differences between the S and Ku bands. For example, the amplitude of the Vostok height variations, where the accumulation of snow is less than  $10 \text{ cm yr}^{-1}$  (Vaughan et al., 1999), are more than 30 cm at Ku band and 70 cm at S band.

We model the compaction rate by letting the surface density  $\rho_0$  vary, and further by adjusting the density profile between the surface and 10 m as described in Section 4.6. The compaction affects the surface signal the most, because of the greater change of dielectric contrast at the air/snow surface.

The waveform parameters are simulated for varying  $\rho_0$  and different surface roughness at Ku and S bands (Fig. 17). The behaviour observed here matches the observations (Fig. 2), that is, a density increase has a positive impact on the backscatter coefficient and a negative one on the leading edge width and the trailing edge slope. The modelled amplitudes are always higher at S band than at Ku band, which is in good agreement with the observations (Figs. 6, 7, 8). This is explained by the fact that the surfaces are smoother at S band, and so, are the main contributions to the S band signal. We also note that the model provides good estimates of the observed amplitude values for seasonal variations.

In summary, snow compaction is the best explanation for the observed seasonal variations. A snow compaction of  $100 \text{ kg m}^{-3}$  as observed by Qin and Young (1988) can explain retracked altitudes variations of up to 0.8 m at Ku band and 1.5 m at S band (Fig. 17). These figures must be compared to the amplitudes found on the Antarctica plateau, that vary from 0 to 70 cm at Ku band and 0 to 1.5 m at S band. The observed cycle in the retrieved height is then caused by the change in the snow surface density, which modifies the altimetric waveform.

The snow compaction hypothesis is also emphasized in the observation of the phase of the signal (Fig. 9). The modelling of Li Jun and Zwally (2002, 2004) suggested that the peak in

compaction rate occurs at different times of the year depending mostly on the accumulation rate and the heat-vapour transfer. We observed in Fig. 9 that the phase changes from the early summer in East Antarctica toward early winter in the dome regions. The compaction theory is thus in good agreement with the observations.

## 7. Conclusion

Since the launch of ENVISAT in 2002, two altimetric datasets are available over the Antarctic ice-cap at two different frequencies at Ku and S bands. We use these new observations, to retrieve shallow snowpack properties. This study focuses on a model of the altimeter echo and the analysis of the seasonal variations of the altimetric signal.

Here we describe a new model which is essential for two main reasons: 1/ existing altimetric models are not adapted to a multiple frequency dataset comparison, and 2/ the dual-frequency radar dataset of ENVISAT over Antarctica shows evidence of small-scale roughness effects on the altimetric signal. The model, based on the classic Brown model (1977) is adapted using an IEM Method (Fung, 1994) to describe the interaction between the radar wave and the snow surface. Both layering and scattering effects in the Ku and S bands are taken into account, by the summation of attenuated surface echoes and an improved Rayleigh scattering method (Mätzler, 1998).

The model reproduces the waveform shapes simultaneously in the two radar bands of ENVISAT. The analysis of the model outputs show the primary importance of the surface micro-roughness effects on the ENVISAT signal, with a strong sensitivity of the backscattering coefficient and the trailing edge slope to this parameter. Smooth surfaces are associated with large backscattering coefficients and low trailing edge slopes. The notion of roughness depends on the incident wave frequency; snow surfaces are smoother at S band than at Ku band. The recurrence of “low TeS, high  $\sigma_0$ ” is greater at S band than at Ku band. At Ku band, snow surfaces are mostly rough associated with a low surface backscatter. This low surface signal favours a better sensitivity of the waveforms to the sub-surface signal and therefore increases the values of the trailing edge slope.

The analysis of the 4 year-time-series of ENVISAT shows that the whole altimetric signal varies seasonally with varying amplitudes over the ice-sheet. The amplitudes are found to be higher for the S band, and all of the parameter variations are well correlated. These seasonal variations have already been observed before in the altimetric data but only in the retrieved altitude (Zwally & Li Jun, 2002). These variations are typically explained through the decrease of the snowpack height by compaction. However snow compaction cannot explain height variations which exceed the amount of precipitation, which is sometimes observed. The temperature cycle effect was investigated first, and does not impact on the S band signal, but instead affects the altitude cycle of the Ku signal to a few 10 s of centimetres. The investigation of the seasonal compaction of the snow explains the observed variations extremely well. The modelling studies show that the change in surface density without any real change in height can explain the observed height variations in the altimetric signal (between 0 and

70 cm at Ku band). These altitude variations are thus an artefact of the retracking algorithm, caused by the sensitivity of the radar waveforms to the density of the snow surface. This conclusion is in opposition with a previous hypothesis (Zwally & Li Jun, 2002) that consider the seasonal variations in retrieved height to be created by a real change of the altitude. Moreover, the amplitudes of the seasonal variations are highly dependent on the shallow snow properties, and particularly on the snow surface roughness. So, these seasonal variations can provide interesting information about the properties of the snowpack.

Recent modelling studies (Li Jun et al., 2007) have shown that changes of the snowpack compaction rate also occur at decadal scales, possibly affecting the altimeter signal. The general trend in the waveform parameters over 4 years has not been studied here. However, a preliminary analysis of the waveform parameter trends shows exactly the same behaviour as for the seasonal variations. This probably indicates that a bias also exists in the altitude retrieved by altimetry over the Antarctic ice-sheet at interannual time scales, due to the interaction of the radar signal with the snowpack properties. This result shows the urgent need to correct the altitude time-series for changes in the waveform shape, as presented by Legrésy et al. (2006) using all of the waveform parameters. Due to their different sensitivity to the snow properties (e.g. the S band signal is not sensitive to the temperature or grain size changes), the dual S and Ku bands are very promising for this type of correction.

Finally, the dual-frequency ENVISAT altimeter is very useful for the study of the snow properties over Antarctica. The S and Ku frequencies have different interactions with the sub-surface properties of the snowpack due to their different penetration properties and their interaction with the snow surface roughness. The model simulations provide a good fit to these signals. The inversion of the dual-frequency dataset of ENVISAT will be the natural continuation of this work.

## Acknowledgements

This work is a contribution to the RAIES ENVISAT RA-2 and OSCAR projects. This work benefits from the comments of two anonymous reviewers. The authors would like to thank Ben Galton-Fenzi and Rosemary Morrow for reviewing the English, and Arthur H. for his support.

## References

- Adams, R. J., & Brown, G. S. (1998). A model for altimeter returns from penetrable geophysical media. *IEEE Transactions on Geoscience and Remote Sensing*, 36, 5.
- Arthern, R. J., Wingham, D. J., & Ridout, A. L. (2001). Controls on ERS altimeter measurements over ice sheets: Footprint-scale topography, backscatter fluctuations, and the dependence of microwave, penetration depth on satellite orientation. *Journal of Geophysical Research*, 106(D24), 33,471–33,484.
- Beckmann, P., & Spizzichino, A. (1987). The scattering of electromagnetic waves from rough surfaces. Norwood, MA: Artech House, Inc. 511 pp.
- Brown, G. S. (1977). The average impulse response of a rough surface and its applications. *IEEE transactions on antennas and propagation*, 25, 1.
- Davis, C. H., & Moore, R. K. (1993). A combined surface and volume-scattering model for ice-sheet radar altimetry. *Journal of Glaciology*, 39(133), 675–686.
- Femenias, P., Rémy, F., Raizonville, R., & Minster, J. F. (1993). Analysis of satellite-altimeter height measurements above continental ice-sheets. *Journal of Glaciology*, 39(133), 591–600.
- Frezzotti, M., Bitelli, G., de Michelis, P., Deponti, A., Forieri, A., Gandolfi, S., et al. (2005). Geophysical survey at Talos Dome (East Antarctica): The search for a new deep-drilling site. *Annals of Glaciology*, 39, 423–432.
- Fung, A. K. (1994). *Microwave Scattering and Emission Models and Their Applications*. Artech House: Boston, MA.
- Fung, A. K., Li, Z., & Chen, K. S. (1992). Backscattering from a randomly rough dielectric surface. *IEEE Transactions on Geoscience and remote sensing*, 30, 2.
- Gerland, S., Oerter, H., Kipfstuhl, J., Wilhelms, F., Miller, H., & Miners, W. D. (1999). Density log of a 181 m long ice core from Berkner Island, Antarctica. *Annals of Glaciology*, 29(1), 215–219 (5).
- Goodwin, I. D. (1988). Firn core data from shallow drilling investigations in eastern Wilkes Land, East Antarctica. *ANARE Research Notes*, 65, 75.
- Gow, A. J. (1968). Deep core studies of the accumulation and densification of snow at Byrd Station and Little America V, Antarctica. *Research report, vol. 197*. U.S. Army Materiel Command, Cold Regions Research and Engineering Laboratory.
- Hawley, R. L., Morris, E. M., Cullen, R., Nixdorf, U., Shepherd, A. P., & Wingham, D. J. (2006). ASIRAS airborne radar resolves internal annual layers in the dry-snow zone of Greenland. *Geophysical Research Letters*, 33, L04502. doi:10.1029/2005GL025147
- Jackson, T. J., McNairn, H., Weltz, M. A., Brisco, B., & Brown, R. (1997). First order surface roughness correction of active microwave observations for estimating soil moisture. *IEEE transactions on geoscience and remote sensing*, 35, 4.
- Jezeq, K. C., Kenneth, C., & Alley, R. B. (1988). Effect of stratigraphy on radar altimetry data collected over ice sheets. *Annals of Glaciology*, 11, 60–63.
- King, J. C., & Turner, J. (1987). *Antarctic Meteorology and Climatology*: Cambridge University Press.
- Lacroix, P., Legrésy, B., Coleman, R., Dechambre, M., & Rémy, F. (2007). Dual-frequency altimeter signal from Envisat on the Amery ice-shelf. *Remote Sensing of Environment*, 109, 285–294.
- Lacroix, P., Legrésy, B., Langley, K., Hamran, S.E., Kohler, J., Roques, S., et al., (submitted for publication), In situ measurements of snow surface roughness using a laser profiler device, *Journal of Glaciology*.
- Langley, K., Hamran, S. E., Hogda, K. A., & Storvold, R. (2007). Use of C-band Ground Penetrating Radar to determine backscatter sources within glaciers. *IEEE Transactions on Geoscience and Remote Sensing*, 45, 1236–1246.
- Langley, K., Lacroix, P., Hamran, S.E., Brandt, O., (submitted for publication), Source of C-band backscatter from the superimposed ice and firn area revealed by multi-frequency GPR and cores, *Journal of Glaciology*.
- Legrésy, B., Papa, F., Rémy, F., Vinay, G., Van den Bosh, M., & Zanife, O. Z. (2005). ENVISAT radar altimeter measurements over continental surfaces and ice caps using the ICE-2 retracking algorithm. *Remote Sensing of Environment*, 95, 150–163.
- Legrésy, B., & Rémy, F. (1997). Surface characteristics of the Antarctic ice sheet and altimetric observations. *Journal of Glaciology*, 43(14), 265–275.
- Legrésy, B., & Rémy, F. (1998). Using the temporal variability of the radar altimetric observations to map surface properties of the antarctic ice sheet. *Journal of Glaciology*, 44(147), 197–206.
- Legrésy, B., Rémy, F., & Blarel, F. (2006). Along track repeat altimetry for ice-sheets and continental surface studies. *Proceedings of the Symposium on 15 years of Progress in Altimetry, Venice ESA-SP614*, paper 181.
- Leushen, C., Clifford, S., & Gogineni, P. (2003). Simulation of a surface-penetrating radar for Mars exploration. *Journal of Geophysical Research*, 108, E4.
- Li Jun, & Zwally, H. J. (2002). Modelled seasonal variations of firn density induced by steady-state surface air-temperature cycle. *Annals of Glaciology*, 34, 299–302.
- Li, Jun, & Zwally, H. J. (2004). Modeling the density variation in the shallow firn layer. *Annals of Glaciology*, 38(1), 309–313.
- Li, Jun, Zwally, H. J., & Comiso, J. C. (2007). Ice-sheet elevation changes caused by variations of the firn compaction rate induced by satellite-observed temperature variations (1982–2003). *Annals of Glaciology*, 46, 8–13.

- Matsuoka, T., Fujita, S., & Mae, S. (1996). Effect of temperature on dielectric properties of ice in the range 5–39 GHz. *Journal of Applied Physics*, 80(10), 5884–5890.
- Mätzler, C. (1998). Improved Born approximation for scattering of radiation in a granular medium. *Journal of Applied Physics*, 83(11), 6111–6117.
- Newkirk, M. H., & Brown, G. S. (1996). A waveform model for surface and volume scattering from ice and snow. *IEEE Transactions on Geoscience and Remote Sensing*, 34, 2.
- Oveisgharan, S., & Zebker, H. A. (2007). Estimating snow accumulation from InSAR correlation observations. *IEEE Transactions on Geoscience and Remote Sensing*, 45(1), 10–20.
- Qin, D., & Young, N. W. (1988). Characteristics of the initial densification of snow/firn in Wilkes Land, East Antarctica. *Annals of Glaciology*, 11, 209.
- Rees, W. G., & Arnold, N. S. (2006). Scale-dependent roughness of a glacier surface: Implications for radar backscatter and aerodynamic roughness modelling. *Journal of Glaciology*, 52(117), 214–222.
- Rémy, F., Legrésy, B., & Testut, L. (2001). Ice sheet and satellite altimetry. *Surveys in Geophysics*, 22(1), 1–29.
- Rémy, F., Schaeffer, P., & Legrésy, B. (1999). Ice flow physical processes derived from the ERS-1 high resolution map of the Antarctica and Greenland ice sheets. *Geophysical Journal International*, 139(3), 645–656.
- Ridley, J. K., & Partington (1988). A model of satellite radar altimeter return from ice-sheets. *Int. J. Remote Sensing*, 9(4), 601–624.
- Surdyk, S., & Fily, M. (1993). Comparison of the passive microwave spectral signature of the Antarctic ice-sheet with ground traverse data. *Annals of Glaciology*, 17, 161–166.
- Tiuri, M. E., Sihvola, A. H., Nyfors, E. G., & Hallikainen, M. T. (1984). The complex dielectric constant of snow at microwave frequencies. *IEEE Journal of Oceanic Engineering*, OE-9(5), 377–382.
- Turner, J., Connolley, W. M., Leonard, S., Marshall, G. J., & Vaughan, D. G. (1999). Spatial and temporal variability of net snow accumulation over the Antarctic from ECMWF re-analysis project data. *International Journal of Climatology*, 19, 697–724.
- Ulaby, F. T., Moore, R. K., & Fung, A. K. (1982). Microwave remote sensing. vol.2. Reading, MA: Artech House.
- Van den Broeke, M. R., & Van Lipzig, N. P. M. (2003). Factors controlling the near-surface wind field in Antarctica. *Monthly Weather Review*, 131, 733–743.
- Vaughan, D. G., Bamber, J. L., Giovinetto, M., Russell, J., & Cooper, A. P. (1999). Reassessment of net surface mass balance in Antarctica. *Journal of Climate*, 12, 933–946.
- West, R. D., Winebrenner, D. P., Tsang, L., & Rott, H. (1996). Microwave emission from density-stratified Antarctic firn at 6 cm wavelength. *Journal of Glaciology*, 42(140), 63–76.
- Wiesman, A., & Matzler, C. (1999). Microwave emission model of layered snowpacks. *Remote Sensing of Environment*, 70, 307–316.
- Wingham, D. J. (1995). A method for determining the average height of a large topographic ice sheet from observations of the echo received by a satellite altimeter. *Journal of Glaciology*, 41(137), 125–141.
- Zribi, M., Ciarletti, V., & Taconet, O. (2000). Validation of a rough surface model based on fractional Brownian geometry with SIRC and ERASME radar data over Orgeval. *Remote Sensing of Environment*, 73(1), 65–72.
- Zwally, H. J., & Li, Jun (2002). Seasonal and interannual variations of firn densification and ice-sheet surface elevation at the Greenland summit. *Journal of Glaciology*, 48(161), 199–207.
- Zwally, H. J., Giovinetto, M. B., Jun, Li, Cornejo, H. G., Beckley, M. A., Brenner, A. C., et al. (2005). Mass changes of the Greenland and Antarctic ice sheets and shelves and contribution to sea-level rise: 1992–2002. *Journal of Glaciology*, 51(175), 509–527.